CHAPTER II

Experimental Methods and Theoretical Background

2.1. Introduction:

The plan of this work is to develop liquid crystalline materials with broad operating temperature range, large negative dielectric anisotropy, low values of optical birefringence and low rotational viscosity for their application in Vertically Aligned mode Liquid Crystal Displays (VA-LCD's) [1-4]. For VA-LCD's, the switching behaviour requires liquid crystal materials with negative dielectric anisotropy ($\Delta\varepsilon < 0$) [5]. Liquid crystalline molecules with lateral polar groups fulfill this requirement. Materials suitable for VA-LCD's are mainly focused on dielectrically negative fluorinated liquid crystals comprising of 1, 2-difluorobenzene building block [6] which combine the necessary polarity with chemical stability and low polarizability [7, 8]. Furthermore, laterally fluorinated terphenyl derivatives have been found to be promising candidates for VA mode applications with improved values of the rotational viscosity, keeping the birefringence in the desired range [9]. Since, no single liquid crystal material can fulfill all the above-mentioned requirements; multi component mixtures with optimum values of the material properties were carefully prepared. Initially Polarizing Optical Microscopy (POM) studies were undertaken for identification of the phases and phase transition temperatures of the pure compounds as well as their mixtures. Differential Scanning Calorimetry (DSC) measurements were done for the determination of the transition enthalpies. The specific work done includes the

preparation of multicomponent mixtures from suitably selected pure components and optimization of their physical properties from optical birefringence (Δn), dielectric anisotropy ($\Delta\varepsilon$), bend elastic constant (K_{33}) and rotational viscosity (γ_1) measurements. Moreover, the effect of the pretilt angle [10-13] on the threshold voltage and the rotational viscosity of the mixtures were also studied. Again, since the order parameter in liquid crystals is one of the most important physical parameters [14-16] which dictate its performance in display devices, therefore the temperature dependence of the Orientational Order Parameter (OOP) were determined from x-ray diffraction studies (on a few selected compounds) and birefringence measurements. The experimentally determined OOP values were compared with the existing theories [17, 18]. Furthermore, since the role of bicyclohexane compounds with low values [19] of the birefringence is definitely important in the optimization of the properties of the final mixtures, therefore the physical properties of a few such compounds have been investigated from optical transmission, birefringence, density and dielectric anisotropic measurements.

2.2. Formulation of multi-component mixtures and construction of phase diagram:

Seven multicomponent mixtures (mixtures **A**, **B**, **C**, **D**, **E**, **F** and **G**) with negative dielectric anisotropy ($\Delta\varepsilon < 0$) were prepared. For mixture preparation the choice of the pure compounds was decided on the basis of their physical properties.

While preparing multicomponent mixtures the eutectic ones are of special interest [20], because they exhibit liquid crystalline mesophase over a broad range of temperature. The melting points of such mixtures are lower than the melting points of the individual components and the clearing points are

intermediate between them, resulting in an increase in the mesomorphic range, as shown in Figure 2.1.

The composition of the eutectic mixture was determined from the Schröder van Laar equation [21, 22]:

$$\ln x_k = -\frac{\Delta H_m^k}{R}\left(\frac{1}{T} - \frac{1}{T_m^k}\right) \qquad (2.1)$$

under the condition,

$$\sum_{k=1}^{n} x_k = 1 \qquad (2.2)$$

where, x_k is the molar ratio of k^{th} component, ΔH_m^k and T_m^k are respectively the melting enthalpy (in J mol^{-1}) and the melting temperature (in K) and R is the universal gas constant (8.31 J mol^{-1} K^{-1}). The lower the melting points and melting enthalpies of the pure components lower is the melting point of the eutectic mixture. When the components show polymorphic phase transitions below their melting points, the equation is more complicated [20], but such compounds are not commonly used.

The compounds were chosen in such a way that, the calculated melting temperature is within a desired range. The mixtures were prepared as per the calculated composition and their melting temperature was determined with the help of a polarizing optical microscope and a hot stage. The experimentally obtained melting point was compared with the calculated melting point. If the difference in both the temperatures exceeded a few degrees, it means that a component may be forming an intermolecular complex and hence it must be removed from the mixture. The calculations and preparation of mixtures were repeated in order to discard the badly soluble compounds.

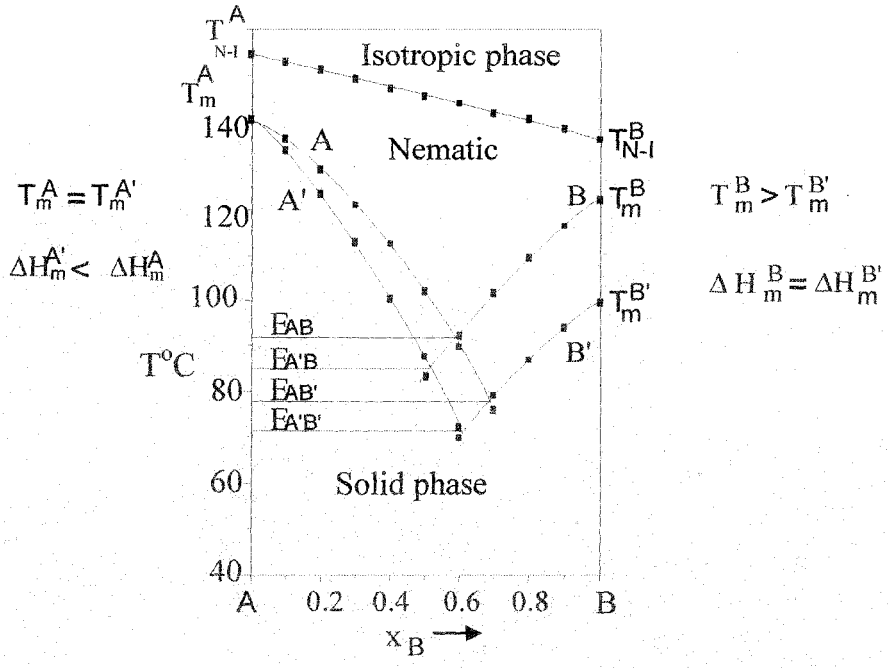

Figure 2.1. The position of eutectic point E for the bicomponent mixture A and B, where ΔH^A_m, ΔH^B_m and T_m^A, T_m^B are the melting enthalpies and melting temperatures of components A and B respectively [23].

This method occasionally predicts the mole fractions of the eutectic mixtures fairly well, but because ideal behavior rarely exists, it can only be used as a guide. Other experimental methods have also been suggested [23]. Generally, experience and experiment are required to obtain low melting point mixtures.

Materials of low melting temperature, low enthalpy of melting and modest nematic range were used as the main components to prepare the base mixture. Care was taken to avoid the formation of induced smectic phases, sometimes observed in polar-non-polar mixtures [24-30]. To this base mixture, materials with a very large negative $\Delta\varepsilon$ were added for obtaining low threshold voltages. The choice of these components was also governed by the required birefringence. It is usually necessary to increase the T_{NI} of the mixture using additives having a high T_{NI} value. The rotational viscosity (γ_1) should be kept

as low as possible to allow fast switching. Hence materials with low rotational viscosity were chosen. In addition, for VA mode displays, mixtures with smaller value of bend elastic constants are targeted. Thus a multi component mixture, containing a wide variety of components, each one contributing to the final properties of the mixture was produced.

The mixtures were prepared using an analytical balance (Mettler Toledo AB-265-S). Texture studies of the liquid crystal compounds was done under a polarizing optical microscope (Motic Research Microscope BA300 with polarising attachment) equipped with a Mettler Thermosystem (FP 900) and a Mettler hot stage (FP-82 HT) with a temperature accuracy of ± 0.1°C for identification of the mesophase and to obtain the phase transition temperatures. The theoretically estimated values of the melting temperature (T_m) and clearing temperature (T_{NI}) of the mixtures at the eutectic composition were compared with those determined experimentally from texture and DSC studies.

2.3. Texture studies:

The most striking feature of the liquid crystals is the wide variety of the visual patterns they display under polarized light. These patterns, called textures, are almost entirely due to the defect structure that occurs in the long range molecular order of the liquid crystalline materials. Appearing under the polarizing microscope as ellipses, parabolas, hyperbolas, lines and points, colorful structural singularities are understood through topological and geometrical arguments. Texture study is an important technique for the determination of the transition temperatures and preliminary phase identification. However, classification of different liquid crystalline phases by observation of the textures alone is often ambiguous, and other methods are required to support it. Detailed description of various textures with photographs is given by Demus and Richter [31].

The liquid crystalline samples were inserted between a glass slide and a cover slip and placed in a hot stage (Mettler FP-82 HT) the temperature of which was controlled by Mettler Thermo System (FP 900). The textures of the phases were observed using a polarizing optical microscope (Motic Research Microscope BA300 with Polarizing Attachment) and the phase transition temperatures were recorded.

2.4. Differential Scanning Calorimetry (DSC):

Differential Scanning Calorimetry (DSC) measurements of the pure compounds were performed to determine the transition enthalpies using a SETARAM 141 calorimeter at the Department of Chemistry, Military University of Technology, Warsaw, Poland. The DSC scans of a few selected compounds were also done at the Department of Chemistry, University of North Bengal using a Perkin Elmer Pyris 6 Differential Scanning Calorimeter calibrated with indium standard.

2.5. Dielectric permittivity measurements:

The static dielectric permittivities $\varepsilon_{\parallel}$ and $\varepsilon_{\perp}$ along and perpendicular to the molecular long axis respectively and hence the dielectric anisotropy $\Delta\varepsilon$ (= $\varepsilon_{\parallel} - \varepsilon_{\perp}$) were determined at 1 kHz by measuring the capacitance of a cell (thickness 8.9μm, procured from AWAT Co. Ltd., Warsaw) with and without the liquid crystalline compound using Agilent E4980A digital LCR-bridge with a relative accuracy of 0.05% [32]. The liquid crystalline material was filled inside a homeotropically aligned cell by capillary action. The cell was mounted inside an electrically powered thermostat-block, the temperature of which was controlled within an accuracy of ± 0.1°C by a temperature controller (Eurotherm PID 2404). The stray capacitance was calculated by measuring the capacitance of spectroscopic grade pure benzene and *para*-xylene. If C_0 is the

measured capacitance of the air filled cell, C_a is the capacitance of the empty cell, excluding the stray capacitance C_S, then one can write:

$$C_0 = C_a + C_S \tag{2.3}$$

Now if the cell be filled with a fluid of known dielectric permittivity ε then the measured capacitance can be written as:

$$C = \varepsilon C_a + C_S \tag{2.4}$$

From equation 2.3 and 2.4 the value of C_S has been calculated. Knowing C_S, the dielectric permittivity can be calculated as:

$$\varepsilon = \frac{C - C_S}{C_0 - C_S} \tag{2.5}$$

The accuracy of the setup has been verified by measuring the dielectric constants of 5CB and 7CB, which are close agreement with the values reported in the literature [33]. The temperature variation of the principal dielectric permittivities $\varepsilon_{\parallel}$ and $\varepsilon_{\perp}$ and the dielectric anisotropy have been determined for the pure compounds and mixtures. The details of the experimental procedure for determining the dielectric permittivities have been reported earlier by Prasad and Das [32].

2.6. Optical birefringence measurements:

Most of the nematic liquid crystals are optically uniaxial and strongly birefringent. A uniaxial liquid crystal has two principal refractive indices viz. ordinary refractive index (n_o) and extraordinary refractive index (n_e). The birefringence is defined by the following equation:

$$\Delta n = n_e - n_o \tag{2.6}$$

The first birefringence measurement was made by E. Dorn [34] and its theoretical explanation was given by O.Weiner and H. Zocher [35, 25]. Refractive indices of the smectic phases have also been measured [26-29]. To

evaluate the molecular polarizabilities of the liquid crystal it is necessary to consider the anisotropic internal field that arises due to anisotropic molecular arrangements within the liquid crystals. Hence, in case of liquid crystals the well-known Lorentz-Lorentz formula for isotropic media is replaced by Neugebauer formula [36] or Vuks formula [37]. Saupe and Maier [17] also applied a more elaborate internal field suggested by Neugebauer.

The ordinary and extra ordinary refractive indices were measured in the nematic and smectic liquid crystal phases, and the effective polarizabilities α_o and α_e was calculated using Vuks internal field model [37]. From the polarizability and density data, the Orientational Order Parameter (OOP), $\langle P_2 \rangle$, was calculated as a function of temperature.

Vuks [37] considered that the internal field is independent of orientation, i.e. an isotropic system with different polarizabilities. The principal polarizabilities and refractive indices according to Vuks can be expressed as:

$$\frac{n_o^2 - 1}{\bar{n}^2 + 2} = \frac{4\pi N}{3}\alpha_o \qquad (2.7)$$

$$\frac{n_e^2 - 1}{\bar{n}^2 + 2} = \frac{4\pi N}{3}\alpha_e \qquad (2.8)$$

where, $n^2 = \frac{1}{3}\left(2n_o^2 + n_e^2\right)$, n is the mean refractive index and α_o and α_e can be calculated directly from the refractive index values.

Optical birefringence measurement has been done by the following two methods. In one method, the ordinary (n_o) and the extraordinary refractive index (n_e) was measured by thin prism technique [38] and from the measured values of n_o, n_e the birefringence ($\Delta n = n_e - n_o$) was calculated. The birefringence (Δn) of a few samples was also determined from Optical Transmission (OT) method [39]. The experimental details of these two methods are briefly discussed below.

2.6.1. Thin prism technique:

In the thin prism method, the refractive indices (n_o, n_e) for wavelength λ=632.8 nm was measured within an accuracy of ±0.0006. A hollow prism with refracting angle less than 2° was prepared using glass slides. The temperature of the prism was controlled with an accuracy of ±0.1°C using a specially constructed heater and Eurotherm PID 2404 temperature controller. The heater containing the liquid crystal filled prism was placed between the pole pieces of an electromagnet and a magnetic field of about 0.8T was applied to the liquid crystal filled prism (Figure 2.2). While passing through the aligned sample, a light beam from a He-Ne LASER was split into ordinary and extraordinary beam and two spots were obtained on a screen. The images of the spots were recorded using a digital camera suitably interfaced with a computer. The high resolution digital images so obtained were further processed to locate the position of the center of the spots which was used to determine the ordinary (n_o) and extraordinary (n_e) refractive indices. The prisms were filled with ultrapure, degassed water and the refractive index was measured, where from the angle of the prism was determined.

To prepare the hollow prisms, optically flat glass slides were taken and cut so as to get the desired size of the prism. These slides were then cleaned with detergent and water and treated in an acid mixture (conc. H_2SO_4 + conc. HNO_3) at 60°C for one hour. The slides were then washed with distilled water and then treated further in 1 molar solution of KOH at 60°C for one hour. The slides were further washed thoroughly with distilled water and then with acetone. A thin glass spacer was introduced between one of the vertical edge of the prism so as to get the desired refracting angle which was kept less than 2°. The glass plates were sealed using a high temperature adhesive and after curing were baked for several hours in an oven.

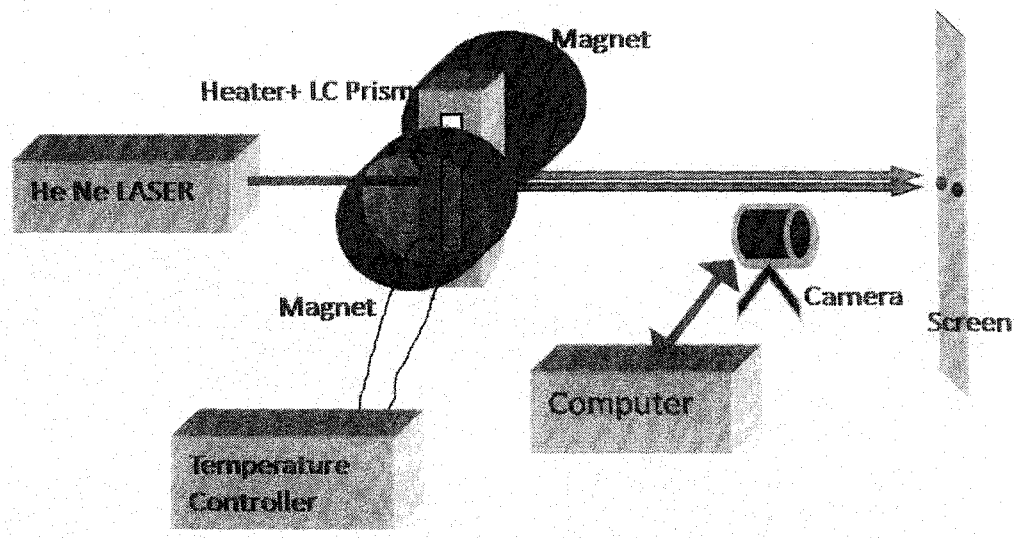

Figure 2.2. Schematic diagram of the experimental set-up for refractive index measurement from thin prism method.

2.6.2. Optical transmission method:

A He-Ne LASER (λ=632.8nm) beam was directed onto an ITO-coated liquid crystal cell of thickness 8.9μm (procured from AWAT Co. Ltd. Warsaw, Poland) placed between two crossed linear polarizers (Figure 2.3). The transmitted light intensity was measured as a function of temperature. The intensity of the transmitted LASER light can be written as [40]:

$$I_t = \frac{\sin^2 2\theta}{2}(1-\cos\Delta\varphi) \qquad (2.9)$$

where, θ is the angle made by the polarizer with the optical axis and the phase difference is given by

$$\Delta\varphi = \frac{2\pi}{\lambda}\Delta nd \qquad (2.10)$$

$\Delta n = n_e - n_o$, where n_e and n_o are the extraordinary and ordinary refractive indices of the liquid crystal medium, and d is the sample thickness. The angle θ was set at 45° to optimize the measurements. The birefringence was calculated from the measured intensity [41, 42]. The output of the digital multimeter and the temperature controller were interfaced with a computer and the

measurements were performed using a suitable program. The details of the experimental set up (Figure 2.3) for the determination of the birefringence from optical transmission studies have been also reported by Prasad and Das [43].

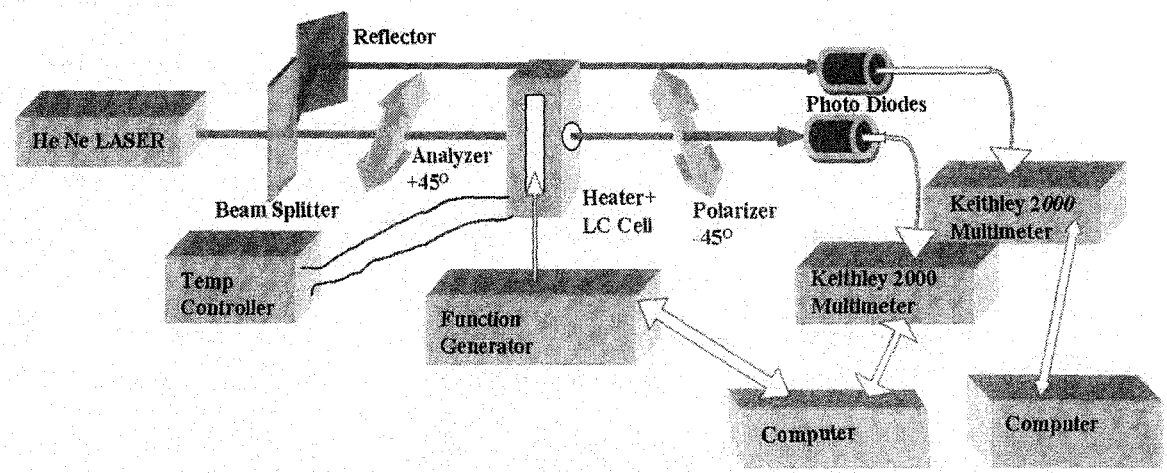

Figure 2.3. Schematic diagram of the experimental set-up for refractive index measurement from optical transmission method.

2.6.3. Determination of Orientational Order Parameter (OOP) from refractive index and optical birefringence measurement:

The relationship between Orientational Order Parameter $<P_2>$ and the principal polarizabilities (α_e, α_o) as given by de Gennes [15] are

$$\alpha_e = \bar{\alpha} + \frac{2}{3}\Delta\alpha_0 < P_2 > \qquad (2.11)$$

$$\alpha_o = \bar{\alpha} + \frac{2}{3}\Delta\alpha_0 < P_2 > \qquad (2.12)$$

where, $\bar{\alpha} = \frac{(2\alpha_o + \alpha_e)}{3}$ is the mean polarizability and $\Delta\alpha_0 = (\alpha_{\parallel} - \alpha_{\perp})$ is molecular polarizability anisotropy, $\alpha_{\parallel}$ and $\alpha_{\perp}$ being the principal

polarizabilities parallel and perpendicular to the molecular long axes in the crystalline state.

From equation 2.11 and 2.12, we obtain

$$< P_2 >= \frac{\alpha_e - \alpha_o}{\alpha_{\parallel} - \alpha_{\perp}} \tag{2.13}$$

To determine the values of $\Delta\alpha_0$ the widely used Haller's extrapolation method [44] was used. For this the polarizability anisotropy in the liquid crystalline state ($\Delta\alpha=\alpha_e-\alpha_o$) was fitted to the equation

$$\Delta\alpha = \Delta\alpha_0\left(1-\frac{T}{T^*}\right)^{\beta} \tag{2.14}$$

where $\Delta\alpha_0$, T^* and β are adjustable parameters.

For a given sample, α_e and α_o were calculated at different temperatures throughout the mesomorphic range. The order parameter $<P_2>$ was calculated using equation 2.13.

Haller's extrapolation method can also be applied directly to the temperature dependence of the birefringence Δn [45, 46] to obtain Δn_0 i.e. the birefringence in the crystalline state. The temperature dependence of the birefringence obtained from optical transmission data is fitted to the following form:

$$\Delta n = \Delta n_0\left(1-\frac{T}{T^*}\right)^{\beta} \tag{2.15}$$

where Δn_0, T^* and β are adjustable parameters. T^* is about 1-3K higher than the clearing temperature. The exponent β depends on molecular structure and its value is close to 0.2. This procedure helps to extrapolate Δn values to the absolute zero temperature, i.e Δn_0 [44].

The order parameter can be obtained directly from the experimental values of temperature dependent birefringence using the relation:

$$<P_2>=\frac{\Delta n}{\Delta n_0} \qquad (2.16)$$

where, Δn_0 is the birefringence in the completely ordered state which was obtained from Haller's extrapolation method [44].

Although this method of determination of order parameter ($<P_2>$) without consideration of the local field experienced by the liquid crystalline molecules has been used by many workers [45-58], the results differ slightly from that obtained if the local field is considered. However, this method is very useful when the density values or the individual values of the refractive indices (n_o, n_e) are not available. Moreover, from the optical transmission method (as described above) high resolution Δn values can be obtained which gives useful information regarding the nature of the phase transitions in these systems.

2.7. Density measurements:

The densities of liquid crystals were measured with the help of a dilatometer of the capillary type. A weighed sample of the liquid crystal was introduced inside the capillary tube of the dilatometer, placed in an insulated glass chamber, the temperature of which was controlled by a temperature controller (Eurotherm PID 2404). Sufficient time was allowed for equilibrium at any desired temperature before taking each reading. The length of the liquid crystal column was measured with a travelling microscope. The densities were calculated after correction for the expansion of glass. The accuracy of the measurement of the densities was within 0.1% [25].

2.8. Elastic constant measurements:

Nematic liquid crystals often consist of long molecules having an average alignment in space which can be described by the unit vector $\hat{n}$, called the director. The bulk free energy per unit volume can be constructed in terms

of the square of the spatial derivatives of the director. For non-chiral systems there are symmetry restrictions on the free energy which limit the possible terms. The terms must be invariant when $\hat{n}$ is replaced by $-\hat{n}$ and linear contributions in the derivatives cannot be allowed since they can change sign if the co-ordinate system is inverted. The resulting free energy integrand has its origins in the works of Zocher [59], Oseen [60, 61] and Frank [62] and is usually called the Frank-Oseen free energy. It can be written in the usual vector notation as:

$$\vec{F}_{def} = \frac{1}{2}\left[\begin{array}{l} K_{11}(\nabla.\vec{n})^2 + K_{22}(\vec{n}.\nabla\times\vec{n})^2 + K_{33}(\vec{n}\times\nabla\times\vec{n})^2 \\ +(K_{22}+K_{44})\nabla.\{(\vec{n}.\nabla)\vec{n} - (\nabla.\vec{n})\vec{n}\} \end{array}\right] \qquad (2.17)$$

where, K_{ii} are the curvature elastic moduli often referred to as the Frank elastic constants. The last term in the right hand side of equation 2.17, sometimes called the saddle-splay term, can be written in the equivalent form $\frac{1}{2}(K_{22}+K_{44})\left[tr\left((\nabla\vec{n})^2 - (\nabla.\vec{n})^2\right)\right]$ when the partial derivatives commute. By considering states of minimum energy in which the director orientation is uniform and everywhere parallel, Ericksen [63] deduced that the elastic constants must satisfy

$$K_{11} > 0, K_{22} > 0, K_{33} > 0 \qquad (2.18)\ (a)$$

$$2K_{11} > K_{22}+K_{44} > 0, K_{22} > |K_{44}| \qquad (2.18)\ (b)$$

And so whilst K_{11}, K_{22} and K_{33} are all positive, K_4 can either be positive or negative.

The saddle-splay term is often omitted since it does not contribute to the bulk equilibrium equations or the boundary conditions for problems involving strong anchoring. Being a divergence its contribution to $\int_V F_{def}\,dv$ can be transformed into a surface integral over the boundary. Neglecting the surface term results in:

$$\vec{F}_{def} = \frac{1}{2}\left[K_{11}(\nabla.\vec{n})^2 + K_{22}(\vec{n}.\nabla\times\vec{n})^2 + K_{33}(\vec{n}\times\nabla\times\vec{n})^2\right] \qquad (2.19)$$

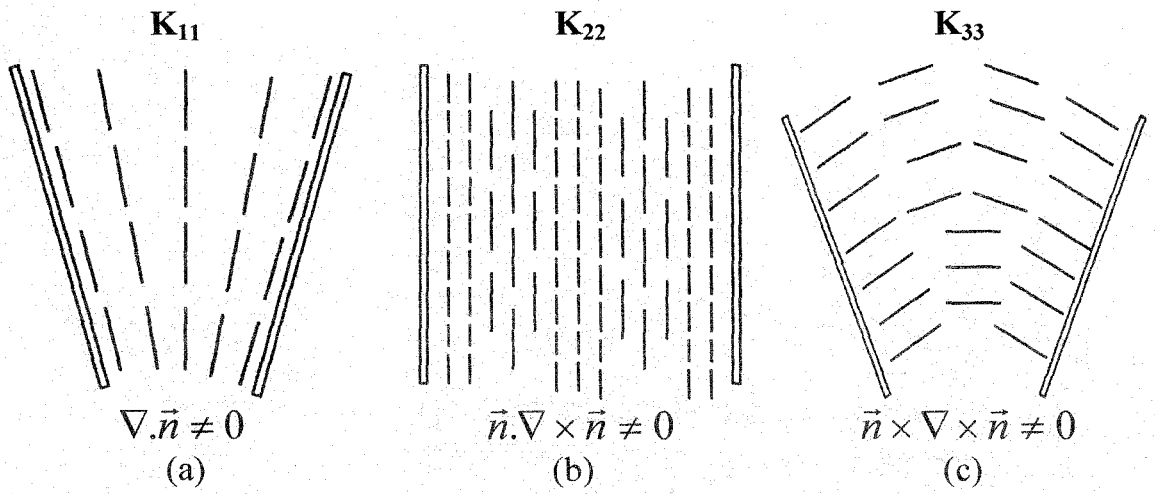

Figure 2.4. The three basic types of distortion in a nematic liquid crystal: (a) splay, (b) twist and (c) bend.

Each term on the right hand side of equation 2.19 represents a specific type of distortion of the director within a given sample of nematic liquid crystal. They are called respectively the splay (K_{11}), twist (K_{22}) and bend (K_{33}) terms and Figure 2.4 schematically shows the possible orientation of $\hat{n}$, indicated by the lines, for each individual distortion: the director orientation is unchanged as one moves vertically through the page. The elastic constants in equation 2.19 have been measured by many experimentalists and are approximately of the order of 10^{-6} dynes (10^{-11} N) with K_{33} often being two or three times larger than K_{11} or K_{22} [64, 15].

The elastic constants of the liquid crystals can be determined by various methods, of which Freedericksz transition [65] is one of the simplest and convenient method. The term Freedericksz transition refers to the deformation of a thin layer of nematic liquid crystal sample with a uniform director pattern in an external electric [66-68] or magnetic field [69-75]. Earlier magnetic field

had been used to observe the Freedericksz transition but recently a new electric field method has been devised using an in-plane electrode configuration [76].

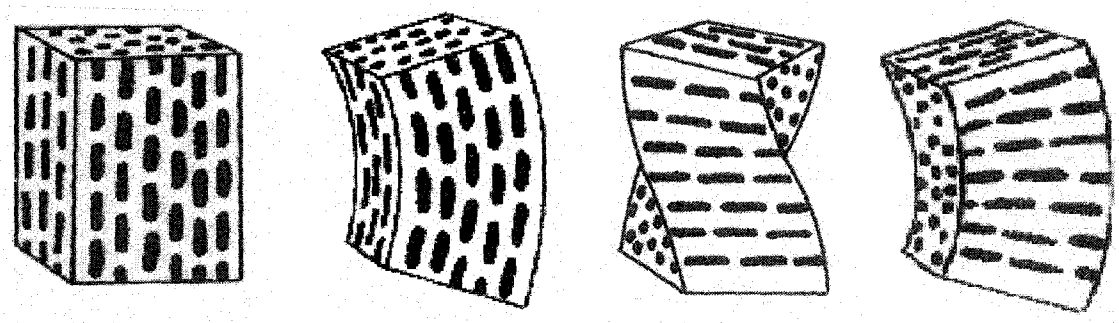

Equilibrium Configuration (a) | Splay (b) | Twist (c) | Bend (d)

Figure 2.5. An ordered liquid crystal in (a) equilibrium configuration. The deformation states are (b) splay, (c) twist and (d) bend.

Freedericksz observed that when a planar surface aligned nematic liquid crystal cell is subjected to electric field normal to the director then the cell undergoes an abrupt change in its optical properties if the strength of the external field exceeds the threshold value, known as the critical field, V_{th}. If the nematic liquid crystals have positive diamagnetic anisotropy or dielectric anisotropy, then as the field exceeds the critical value, the director starts to align along the external field. Depending on the geometry of the arrangement, we can determine, splay, twist or bend elastic constants from Freedericksz transition in the electric field. It is shown schematically in Figures 2.5(b) – 2.5(d).

The bend elastic constants (K_{33}) for the pure compounds and as well as for the mixtures have been determined from electric field induced Freedericksz transition [77]. The cells (procured from AWAT Co. Ltd., Warsaw, Poland) were examined under a polarizing microscope to check the uniformity of the alignment. The temperature of the thermostat was kept constant within ± 0.1°C

during the experiment using a temperature controller (Eurotherm PID 2404). The cells were placed in a brass thermostat with glass windows. The voltage dependence of the capacity of the homeotropically aligned nematic cell (for the bend configuration) was determined at 1 KHz with high precision digital LCR-bridge (Agilent E4980A) from 0 to 20 V_{RMS}. The capacitance of the cell as a function of the applied (sinusoidal) voltage was recorded. The voltage step was 0.02V in the vicinity of the Freedericksz transition and 200mV for the higher voltage. The critical electric field for Freedericksz transition could be observed quite accurately (within 2%) from the sudden change in the capacitance value. The relevant elastic constant was calculated from the well known equation

$$K_{33} = \frac{\varepsilon_0 |\Delta\varepsilon| V_{th}^2}{\pi^2} \qquad (2.20)$$

2.9. Rotational viscosity measurements:

The viscosity of a fluid is a measure of its resistance to fluidic motion. The viscosity at room temperature of a typical nematic liquid crystal is about ten times that of water. Although there is no complete theoretical explanation of the viscosity of liquid crystal materials in relation to their other properties and structure, in an anisotropic fluid, viscosity is best described by a viscosity coefficient tensor which can handle different viscosity values in different directions; and generally, a positive anisotropic liquid crystal having its intrinsic dipole moment aligned with the molecular long axis has a stronger anisotropy and consequently its easier turning makes for a lower viscosity. Viscosity is dependent on temperature exponentially as $\xi = \xi_0 e^{(E/k_\beta T)}$ where, ξ_o is an experimentally derived constant, k_β is the Boltzmann constant and E is the activation energy (the minimum potential energy required for molecular diffusion). It is clear that as the temperature rises, the exponential function $\exp(E/k_\beta T)$ decreases rapidly and therefore the viscosity decreases. Since the

principal operating motion of liquid crystal molecules in displays are rotational, when an external field is turned on, the viscosity is reflected in the coefficient of dynamic rotational viscosity commonly denoted by γ_1. The higher the dynamic rotational viscosity, the slower is the response of the liquid crystal to the electric field.

A relaxation method was used to determine the rotational viscosity, where a small voltage was applied to a homeotropically aligned Liquid Crystal (LC) cell to deform the nematic directors by a small angle [78-82, 74]. At time t = 0, when this voltage is removed, the molecules relax to the equilibrium state with relaxation time (τ_0). For a LC inserted into a homeotropically aligned cell of thickness d, τ_0 is related to the following material parameters

$$\gamma_1 = \frac{\tau_0 K_{33} \pi^2}{d^2} \tag{2.21}$$

where, K_{33} is the bend elastic constant coefficient and γ_1 is the rotational viscosity of the liquid crystal. The bend elastic constants of these mixtures have been determined by us from electric field induced Freedericksz transition [65, 77].

By measuring the transmitted light intensity through a homeotropically aligned LC cell, the optical phase was obtained as a function of time. Assuming that the LC directors are deformed on the application of voltage by a small angle, the decay time is approximated by the following equation [78]:

$$\delta(t) \cong \delta_o \exp(-2t / \tau_o) \tag{2.22}$$

where, δ_0 is the total phase change of the LC cell under a bias voltage V_B. A plot of $\ln[\delta_0/\delta(t)]$ versus time is linear, with a slope equal to $2/\tau_0$, which yields the relaxation time (τ_0). In case, where δ_0 is near the region $N\pi$ (N= integer), $\delta(t)$ becomes $\delta_0 \exp(-4t/\tau_0)$ in the above expression (Equation 2.22).

The schematic representation of the experimental set-up for rotational viscosity measurement is shown in Figure 2.6. A He-Ne LASER (λ = 632.8nm)

was allowed to pass through a homeotropically aligned ITO coated LC cell (procured from AWAT CO, Warsaw, Poland) placed between two crossed polarizers oriented at 45° to the director. The temperature of the cell was regulated and measured by a temperature controller (Eurotherm PID 2404) with an accuracy of ± 0.1°C by placing the cell in a brass thermostat with glass windows. A voltage was applied to the cell and the transmitted light intensity was measured as a function of voltage, using a photodiode. The voltage dependence of the transmitted light intensity exhibited several maxima and minima. A voltage corresponding to the first maximum or minimum in the transmitted intensity was then applied to the LC cell and after sufficient time removed abruptly (Figure 2.7a). The corresponding photodiode output was recorded using a Digital Storage Oscilloscope (DSO). During the relaxation process when the voltage V_B was removed at t = 0, the optical transmission decreases (Figure 2.7(b)) and the phase change δ(t) could be calculated from the time-dependent intensity, I(t), according to the following equation

$$I(t) = I_o \sin^2\{(\Delta_{tot} - \delta(t))/2\} \tag{2.23}$$

where, I_o is the maximum intensity change and $\Delta_{tot} = \frac{2\pi d\Delta n}{\lambda}$ is the total optical phase retardation, which was calculated from precise birefringence measurement. Once δ(t) was determined the relaxation time was ascertained from the slope of the $\ln[\delta_o/\delta(t)]$ versus time plot. Thus by measuring the relaxation time τ_o, and from the knowledge of the bend elastic constant K_{33} and the cell gap d, the rotational viscosity γ_1 was determined.

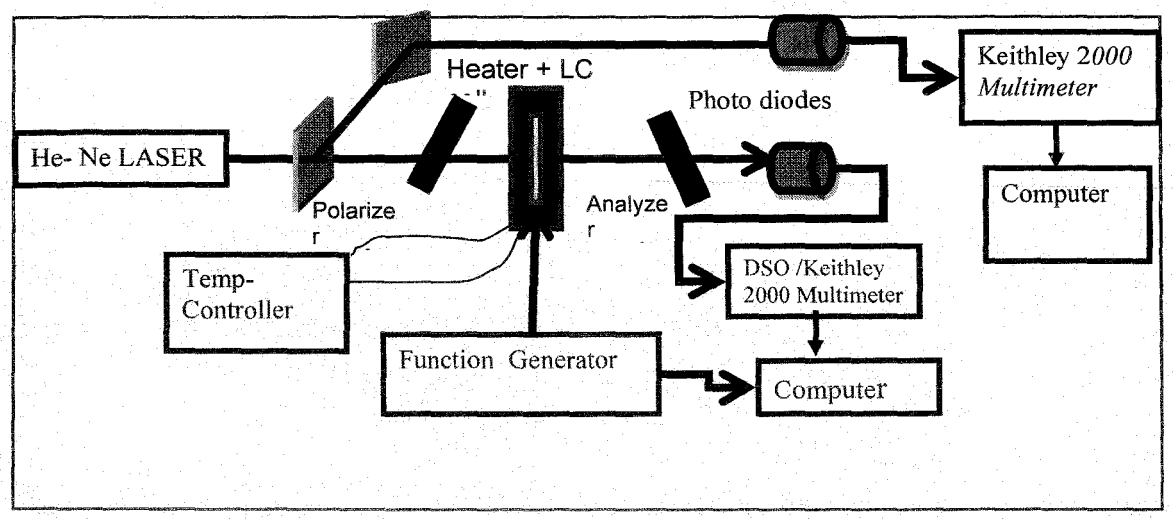

Figure 2.6. Schematic diagram of the experimental set-up for rotational viscosity measurement.

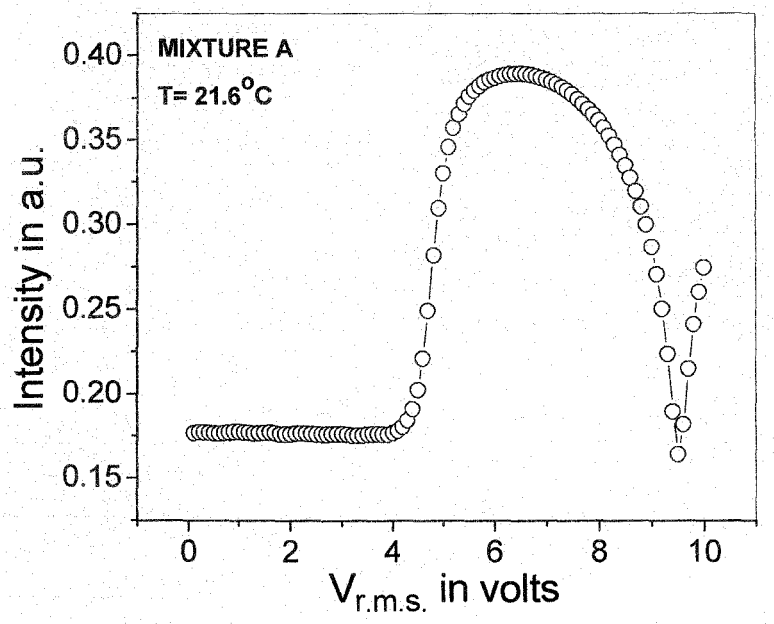

(a)

Figure 2.7. Voltage dependent transmittance of tri-component mixture **A** placed inside a 8.9μm thick homeotropically aligned liquid crystal cell at T= 21.6°C.

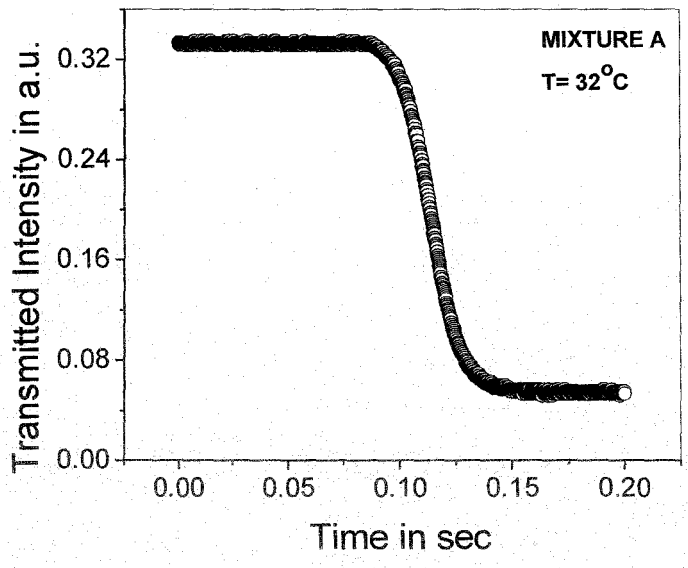

(b)

Figure 2.7. 'contd. Time dependent intensity of mixture **A** at T = 48°C, when bias voltage is removed instantaneously.

2.10. Figure of Merit (FoM) and visco-elastic co-efficient (γ_1/K_{33}):

To compare the performance of a liquid crystal mixture in a display device, a parameter Figure of Merit (FoM) that takes the birefringence and visco-elastic co-efficient (γ_1/K_{33}) into account has been defined as follows [83]:

$$\text{FoM} = (\Delta n)^2 / (\gamma_1 / K_{33}) \qquad (2.24)$$

Each of the three physical properties birefringence (Δn), γ_1/K_{33} and FoM is temperature dependent. FoM is commonly used to assess the performance of a LC compound or mixture because it is independent of the cell gap employed. It is a convenient parameter to compare the switching speed [84] of different compounds. Although birefringence and visco-elastic coefficient can be compared directly, but response time [85] can only be compared if each compound is studied utilizing a cell gap that exactly matches its birefringence in order to obtain the best response time. FoM eliminates the necessity of

matching the cell gap to birefringence as the parameter is independent of cell gap and allows side by side comparison of the performance of different compounds and their mixtures in a device. Moreover, because LC performance and response time is determined by several temperature dependent factors, the FoM values also allow determination of the ideal operating temperature range.

The visco-elastic co-efficient (γ_1/K_{33}) is calculated from the free relaxation time and characterizes the amount of time and energy required to rotate the LC molecules. Since, all of these parameters are temperature dependent, the Figure of Merit (FoM) also strongly depends on the temperature. In the low-temperature region, even though the values of the birefringence, elastic constants and rotational viscosity, all decreases as the temperature increases, the change of the visco-elastic coefficient (γ_1/K_{33}) with temperature is faster than that of $(\Delta n)^2$. Therefore the FoM generally at first increases with increasing temperature and reaches a maximum value at a particular temperature below the nematic-isotropic (N-I) transition temperature, T_{NI}. As the temperature approaches the clearing temperature T_{NI}, the birefringence has a very steep drop, which causes a sharp decrease in the FoM. The higher FoM a liquid crystalline material possess, the faster response time it exhibits. Thus operating a liquid crystal device at an elevated temperature is beneficial for reducing response time. However, it brings complication to the driving scheme by the additional temperature control system.

2.11. Activation energy:

The temperature dependence of γ_1 can be fitted to equation 2.25 to obtain the activation energy [86]:

$$\gamma_1 = \gamma_0 < P_2 > \exp(\frac{E_a}{k_\beta T}) \qquad (2.25)$$

where k_β is the Boltzmann constant, γ_0 is fitting parameter, E_a is the associated activation energy and $\langle P_2 \rangle$ is the Orientational Order Parameter (OOP) obtained from either x-ray diffraction or birefringence measurements.

2.12. Pretilt angle effect:

Pretilt angle [10-13, 87] effect is found to make an important contribution to the liquid crystal dynamics. In a vertically aligned (VA) cell, the pretilt angle (α) affects the device contrast ratio and response time. The pretilt angle is defined as the angle of the LC directors deviated from cell normal. For $\alpha = 0^0$, it implies that the LC directors are aligned perpendicular to the substrate surfaces (Figure 2.8(a)). As the pretilt angle deviates from the cell normal, the Freedericksz threshold voltage is gradually decreased and hence the operating voltage is reduced (Figure 2.8(b)). In fact, in a real LC device a small pretilt angle is required for LC directors to relax back without creating domains.

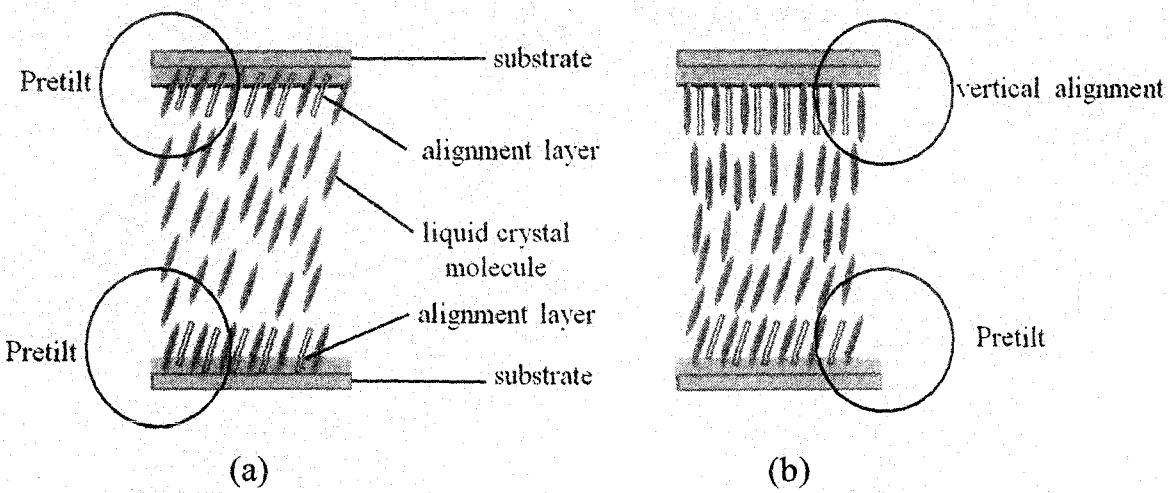

Figure 2.8. Effect of pretilt angle in VA mode nematic LCD: (a) upper and lower substrates with perpendicular and pretitled alignment respectively and (b) uniform pretilt in a LC cell facilitates reduction in the threshold voltage.

From the manufacturer point of view, for a Vertically Aligned Nematic (VAN) display, a delicate balance between response time and contrast has to be maintained. In fact in nematic liquid crystal displays, a slightly pretilted

alignment plays an important role to eliminate orientational defects which further helps us to improve the device quality. However the pretilt has also a drawback: the relaxed state becomes birefringent, and the contrast decays dramatically as pretilt increases. Therefore, choosing a precise pretilt is an important tradeoff when designing real VAN displays.

2.13. X-ray diffraction measurements:

The structure of the liquid crystalline compound can be best understood from the x-ray diffraction studies. Vainshtein [88] and Leadbetter [89, 90] have given the theoretical interpretation of the x-ray diffraction patterns in liquid crystalline materials. From x-ray experiment, the Fourier image of the correlation density function can be determined, the reconstruction of which from the scattered data yields information both on the mutual arrangement of molecules in a liquid crystal and the specific features of the orientational and translational order. Thus the x-ray data enables the statistical functions characterizing various distortions of the initial crystal lattice to be determined [88, 89], and yields the parameters of the orientational order in a liquid crystal, the tilt of the molecules and the electron distribution in the smectic layers [89-93].

X-ray diffraction of the unoriented nematic phase consists of a uniform halo just like that of an isotropic liquid. This is due to the fact that a nematic liquid crystal generally consists of a large number of domains, the molecules being ordered within each domain along the director $\hat{n}$, but there is no preferred direction for the sample as a whole so that the diffraction pattern has symmetry of revolution around the direction of the x-ray beam.

However, application of suitable magnetic or electric field can produce a 'monodomain' or 'aligned' or 'oriented' sample of liquid crystal. The small angle x-ray diffraction pattern from a nematic liquid crystal oriented

perpendicular to the direction of the incident x-ray beam is shown in the Figure 2.9(a). The main halo is split into two crescents for each of which the intensity is maximum along the equatorial direction, i.e. perpendicular to the director. These crescents are formed mainly due to the intermolecular scattering and the corresponding Bragg angle is a measure of lateral intermolecular distance, D. The angular distribution of the x-ray intensity I (ψ) *vs.* ψ curve, also gives the orientational distribution function f(cosθ) and order parameter $\langle P_L \rangle$, (L= 2, 4).

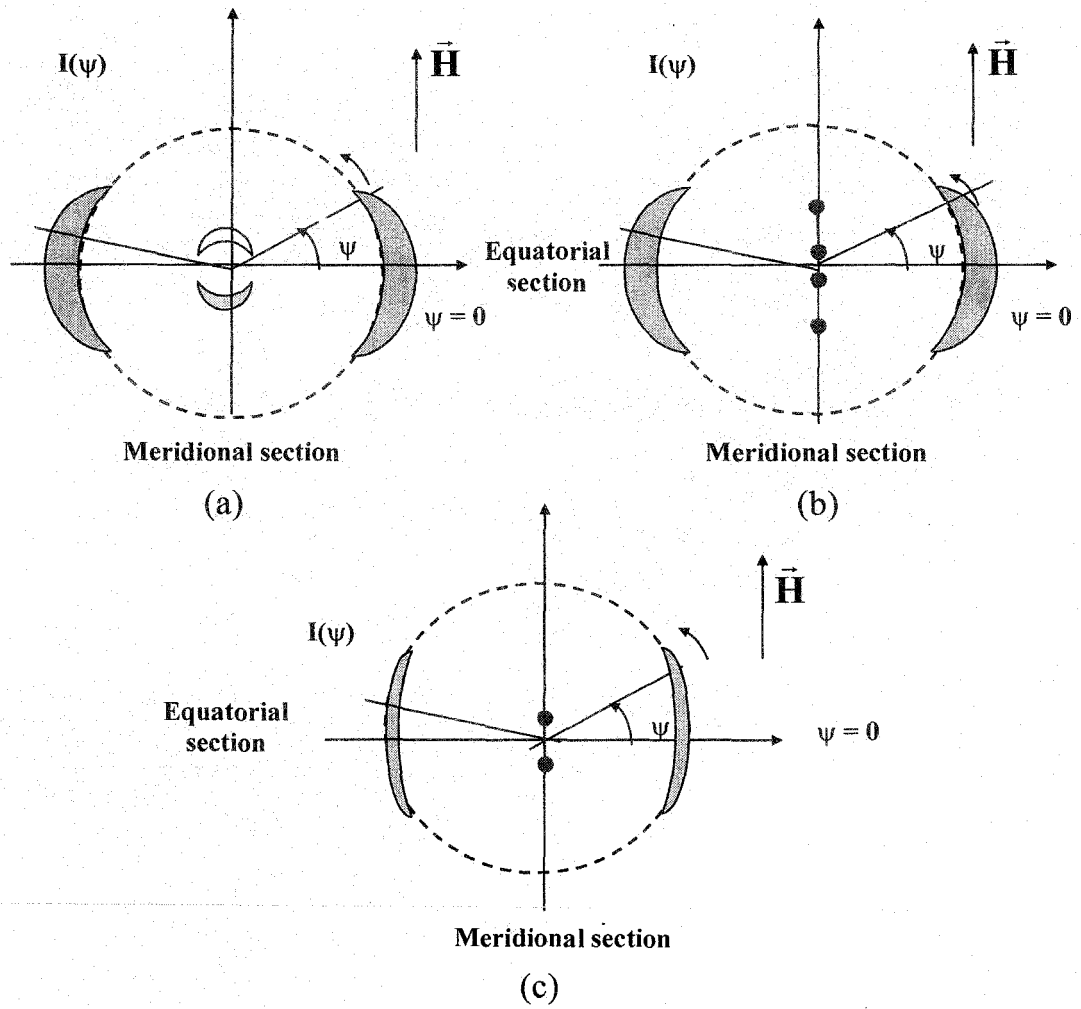

Figure 2.9. Schematic representation of x-ray diffraction pattern of an oriented (a) Nematic, (b) Smectic A and (c) Smectic B phase with the x-ray beam parallel to the layer normal.

The x-ray diffraction setup used in our laboratory has been designed and fabricated by Jha and Paul [94], the schematic diagram of which is given below

(Figure 2.10). The x-ray diffraction patterns of magnetically oriented samples at various temperatures were recorded on a x-ray film in a flat plate camera in the transmission geometry, using Ni filtered Cu K_α radiation of wavelength λ=1.542Å. The collimator of various diameters can be interchanged and the sample to film distance as well as the magnetic field strength can be varied as per requirement.

A vertical x-ray beam is incident on the sample through the collimator, which fits into the sample holder. The sample holder, which is made up of brass has non magnetic heating coils which are insulated by asbestos cement and is held in place by the supporting posts. The holder is well insulated from the posts by asbestos sheets and syndanyo boards. The sample is filled in a thin walled glass capillary of diameter 0.8 mm. The sample holder with the insulation has a thickness of about 2 cm so that the tapering pole pieces of the electromagnet can be brought close together to obtain a magnetic field of about 0.8 Tesla.

The four supporting posts are rigidly attached to a heavy brass plate. The film cassette is mounted on a cassette holder which is also supported by the posts. Spacers can be introduced along the posts between the clamps of the cassette holder and the heavy brass plate so that reproducible geometry can be obtained. Leveling screws can be used for adjustment and improved collimation. The temperature of the sample was regulated within ±0.1 °C by a Eurotherm temperature controller PID 2404. The sample holder was calibrated up to 250°C with a number of samples of known melting points. A gauss meter was used to measure the magnetic field between the pole pieces. For all the photographs, Ni filter of thickness 0.009 mm was used to obtain nearly monochromatic Cu K_α radiation of wavelength λ=1.542Å. The x-ray beam was collimated by a collimator of aperture 1.0 mm. The exact distance between the sample and the film was obtained by taking x-ray diffraction pattern of well characterized samples.

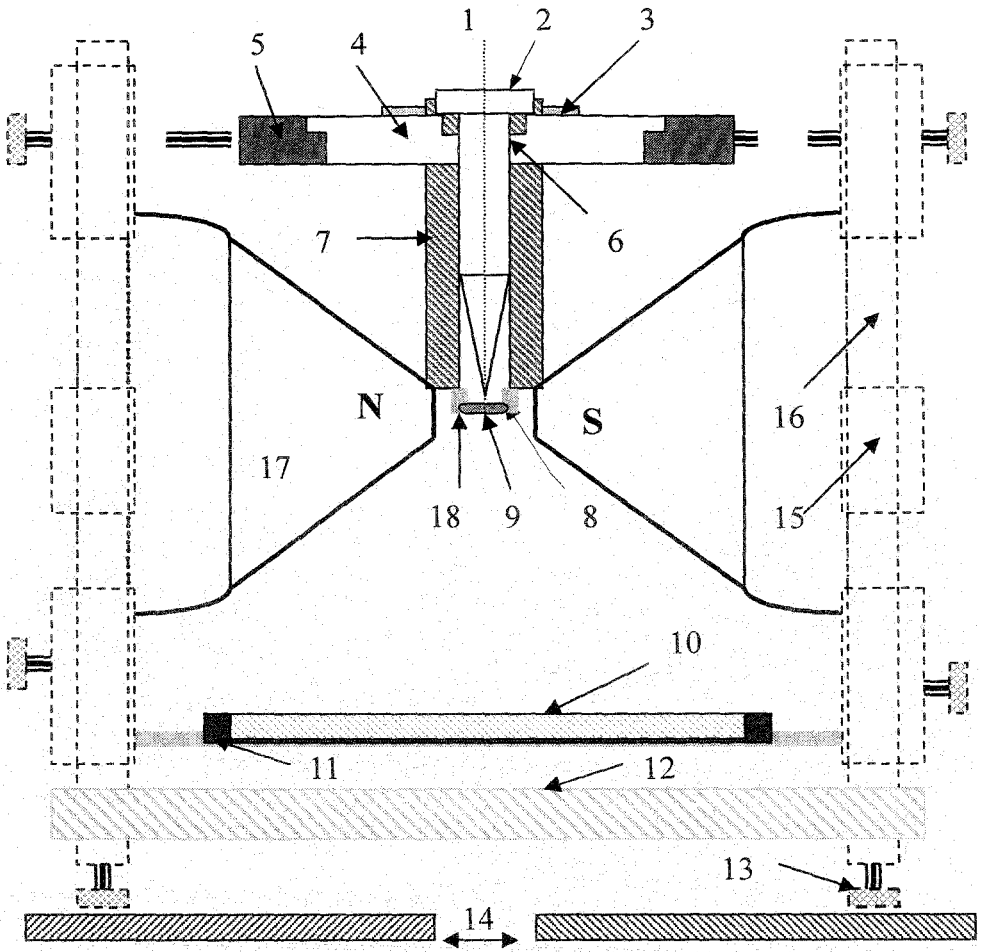

Figure 2.10. Sectional diagram of the x-ray diffraction set-up.

1. X-ray, 2. Collimator, 3. Brass ring, 4. Ring of syndanyo board, 5.Brass ring, 6. Cylindrical brass chamber, 7. Asbestos insulation and heater winding, 8. Specimen holder and thermocouple, 9. Sample position, 10. Film Cassette, 11. Film cassette holder, 12. Base plate, 13. Leveling screw, 14. Brass plates over the coils of the electromagnet, 15. Removable spacer, 16. Supporting brass stand, 17. Pole pieces and 18. Asbestos insulation.

The x-ray photographs were scanned by a high resolution scanner (HP Scanjet 5590) in the gray mode and at 1200 dpi resolution. The optical densities of the pixels were calculated and then converted to x-ray intensities with the help of a calibration curve following the procedure of Klug and Alexander [95]. A program was written in GNU octave to obtain the scattered intensity profile $I(\psi)$ as a function of the azimuthal angle ψ from the x-ray

diffraction photographs (Figure 2.11). All the phases exhibited by the samples under investigation in this work are uniaxial and have a cylindrical symmetry about their long axis. The molecular long axis is oriented about the director $\hat{n}$. The orientational distribution function describes the distribution of the molecular long axis about the director. It gives the probability of finding a molecule at an angle β with respect to the director $\hat{n}$.

The scattered intensity profile I(ψ) (ψ is the azimuthal angle) of the outer diffused equatorial arc is related to the orientational distribution function according to the relation given by Leadbetter and Norris [90]:

$$I(\Psi) = c \int_{\beta=\Psi}^{\pi/2} f_d(\beta) \sec^2 \Psi [\tan^2 \beta - \tan^2 \Psi]^{-1/2} \sin \beta \, d\beta \tag{2.26}$$

where, $f_d(\beta)$ is the distribution function for the orientation β for a local cluster of molecules relative to the director $\hat{n}$ (β = 0). The above equation can be numerically inverted to give $f_d(\beta)$ which is assumed to be close to the singlet distribution function f(β). The Orientational Order Parameter $\langle P_2 \rangle$ and $\langle P_4 \rangle$, defined as the average orientation of the molecular long axes with respect to the director, were calculated using the following equation:

$$\langle P_L \rangle = \frac{\int_0^1 P_L(\cos \beta) f_d(\beta) d(\cos \beta)}{\int_0^1 f_d(\beta) d(\cos \beta)} \tag{2.27}$$

where, L = 2, 4.

To calculate $f_d(\beta)$ and hence the order parameter, I(ψ) values from ψ = 0 to ψ = 90° is required. The I(ψ) values of in the four quadrants were measured separately and the average values of I(ψ) was used to determine f(β), $\langle P_2 \rangle$ and $\langle P_4 \rangle$. The errors in the calculation of $\langle P_2 \rangle$ and $\langle P_4 \rangle$ have been estimated to be less than ± 0.015.

The average lateral distance between the neighbouring molecules (D) is related to the corresponding Bragg angle (2θ) as [92, 93]

$$2D\sin\theta = k\lambda \qquad (2.28)$$

where, 2θ is the Bragg angle for the equatorial diffraction, λ is the x-ray wave length and k is a constant (=1.117 for the perfectly ordered state) which comes from the cylindrical symmetry of the system.

The Bragg equation 2d sinθ =λ (θ is the Bragg angle for the meridional diffraction spots) has been used to calculate the apparent molecular length (l) or layer thickness (d).

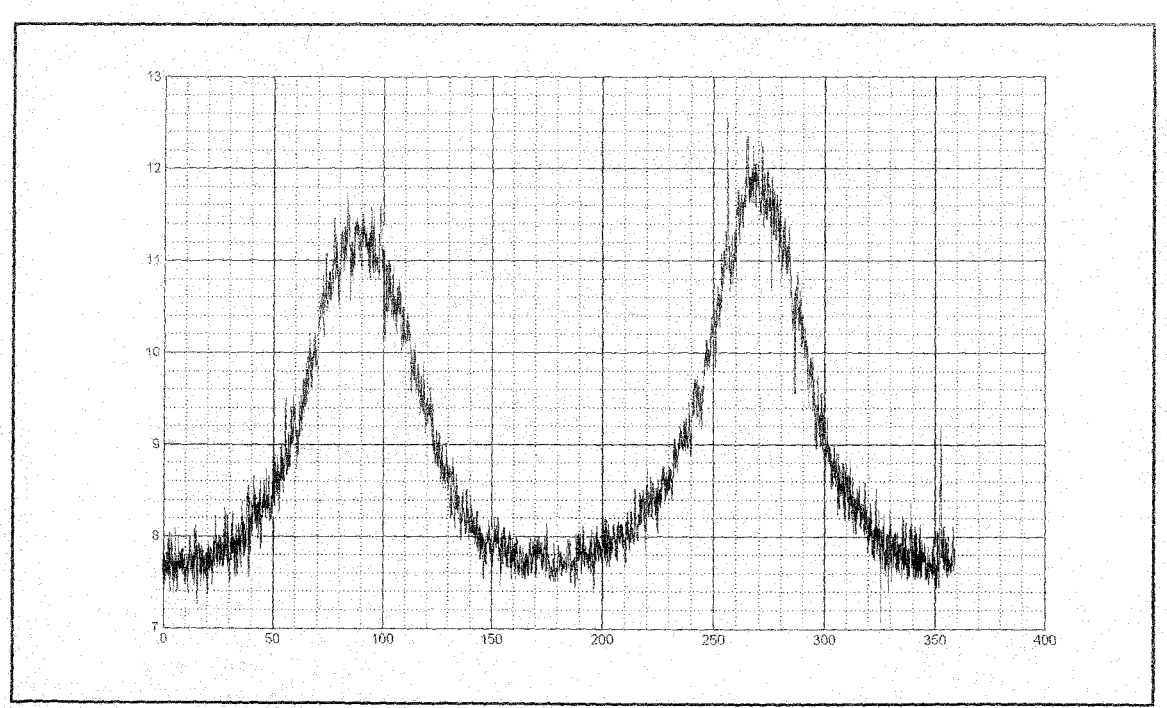

Figure 2.11. Azimuthal scan of the x-ray diffraction film in the nematic phase. Horizontal and vertical axes represent azimuthal angle in degree and x-ray intensity in arbitrary units respectively.

2.14. Theoretical background:

2.14.1. Maier-Saupe theory:

Maier and Saupe [17] have given a molecular statistical theory of the nematic phase (N) and nematic to isotropic (N-I) phase transition. The stability

of the nematic liquid crystal phase arises from the existence of the anisotropic part of the dispersion interaction energy between the molecules. This energy originates from the intermolecular electrostatic interaction. Maier and Saupe approximated the electrostatic interaction by the first term of its multipole expansion and assumed that:

i) the influence of the permanent dipoles can be neglected as far as long range nematic order is concerned.

ii) only the effect of the induced dipole-dipole interaction need to be considered.

iii) the molecules may be considered to be cylindrically symmetric about its long axis.

iv) with respect to a given molecule the distribution of the centre of mass of the remaining molecules may be taken to be spherically symmetric.

The distribution of the molecular long axis about the director is given by an orientational distribution function f(cosθ), wherein θ is the angle between the director and the molecular long axis. As the molecules have no head to tail asymmetry, f(cosθ) is an even function of cosθ. Thus the orientational distribution function can be written as,

$$f(\cos\ \theta) = \sum_{L-even} \frac{(2L+1)}{2} < P_L(\cos\ \theta) > P_L(\cos\ \theta) \quad (2.29)$$

where $P_L\ (\ cos\theta\ )$ are the L^{th} even order Legendre polynomials, and $<P_L\ (cos\ \theta)>$ are the statistical average given by

$$< P_L(\cos\ \theta) >= \int_0^1 P_L(\cos\ \theta) f(\cos\ \theta) d(\cos\ \theta) \quad (2.30)$$

$<P_L>$ are called the Orientational Order Parameters (OOPs). Humphries *et al* [96] has given a more comprehensive concept by including higher order terms in the mean field potential for cylindrically symmetric molecules as,

$$V(\cos\ \theta) = \sum_{L-even} U_L < P_L > P_L(\cos\ \theta) \quad (L\neq 0) \quad (2.31)$$

where U_L are the functions of distance between the central molecule and its neighbours only. Putting Legendre polynomials, L = 2 in equation 2.32 we get,

$$< P_2(\cos\theta) >= \int_0^1 P_2(\cos\theta) f(\cos\theta) d(\cos\theta) \qquad (2.32)$$

$<P_2>$ is generally called the order parameter. For isotropic liquid $<P_2>$ = 0 and for perfectly ordered sample $<P_2>$ =1.

Retaining the first term of the right hand side of equation 2.32, the expression for the potential energy of a single molecule can be written as

$$V(\cos\theta) = -vP_2(\cos\theta) < P_2 > \qquad (2.33)$$

where, $v = -U_2$

The orientational distribution function for a single molecule is given by

$$f(\cos\theta) = Z^{-1} \exp[\, -V(\cos\theta) / kT \,] \qquad (2.34)$$

where Z is the single molecule partition function given by

$$Z = \int_0^1 \exp[\, -V(\cos\theta) / kT \,] d(\cos\theta) \qquad (2.35)$$

and k is the Boltzmann's constant.

Substituting the value of v(cosθ) and f(cosθ) from equation 2.34 and equation 2.35 into equation 2.33 we can write

$$< P_2(\cos\theta) >= \frac{\int_0^1 P_2(\cos\theta) \exp[\, P_2(\cos\theta) < P_2 > / T^*] d(\cos\theta)}{\int_0^1 \exp[\, P_2(\cos\theta) < P_2 > / T^*] d(\cos\theta)} \qquad (2.36)$$

where $T^* = kT / v$

Equation 2.36 is a self-consistent equation. For every temperature T* we can obtain the value of $<P_2>$ that satisfies the self-consistent equation. For normal liquid corresponding to the isotropic state, the value of $<P_2>$ = 0 is a solution at all temperatures. In addition, for temperatures T* < 0.22284, two more solutions of $<P_2>$ appear. It has been found that the nematic phase with

$\langle P_2 \rangle > 0$ is stable when the T* satisfies the condition $0 \leq T^* \leq 0.22019$. With $T^* > 0.22019$, a stable isotropic phase results with $\langle P_2 \rangle = 0$.

The order parameter $\langle P_2 \rangle$ decreases from unity to a minimum value of 0.4289 at T*=0.22019. The nematic - isotropic (N-I) phase transition takes place at T* = 0.22019 and it is of first order, with a discontinuous change of order parameter $\langle P_2 \rangle$ from 0.4289 to 0. However, the energy associated with N-I phase transition is about 0.83 cal/mole-K, which is much smaller than that of usual solid-liquid transition, which is of the order 25 cal/mole-K. These transitions are often called weakly first order transitions. Values of $\langle P_2 \rangle$ as a function of T^* can be calculated easily by solving equation 2.36 iteratively. Although approximations are involved in Maier-Saupe theory, for a number of nematic liquid crystals, the experimental values of $\langle P_2 \rangle$ agree quite well with those predicted by the theory.

2.14.2. McMillan's theory for Smectic A phase:

In smectic A phase, there is a periodic density variation along the layer normal (say, z-direction) in addition to the orientational distribution of the molecular axes. McMillan [18] proposed a simple and elegant description of Smectic A liquid crystal by extending the Maier-Saupe theory to include an additional order parameter for characterizing the one-dimensional translational periodicity of a layered structure. Therefore, the normalized distribution function can be written as:

$$f(\cos\theta) = \sum_{L-even} \sum_{n} A_{L,n} P_L(\cos\theta) \cos\left(\frac{2\pi n z}{d}\right) \tag{2.37}$$

$$\text{with} \quad \int_{-1}^{1} \int_{0}^{d} f(\cos\theta, z)\, dz \quad d(\cos\theta) = 1 \tag{2.38}$$

as normalizing condition, where d is the layer thickness.

McMillan [18] following Kobayashi [97, 98] expressed the pair potential as

$$V_M(\cos\theta, z) = -V[\delta\alpha\tau \cos\left(\frac{2\pi z}{d}\right) + \{\eta + \alpha\delta \cos\left(\frac{2\pi z}{d}\right)\}P_2(\cos\theta) \quad (2.39)$$

where α and δ are the two parameters of the potential. Here, $\eta =< P_2(\cos\theta) >$, $\tau =< \cos\left(\frac{2\pi z}{d}\right) >$ and $\sigma =< P_2(\cos\theta)\cos\left(\frac{2\pi z}{d}\right) >$ are the orientational, translational and mixed order parameters respectively and <····> denotes the statistical average of the quantities inside.

The distribution function can thus be written as

$$f_M(\cos\theta, z) = Z^{-1} \exp[-V_M(\cos\theta, z)/kT] \quad (2.40)$$

where, Z is the single molecule partition function given by

$$Z = \int_0^1 \int_0^d \exp[-V_M(\cos\theta, z)/kT]\, d(\cos\theta)\, dz \quad (2.41)$$

Here also, three self-consistent equations containing η, τ and σ can be written and solved iteratively. Depending on the values of the coupling parameters, the following three solutions are possible:

i) $\eta = \tau = \sigma = 0$, this describes the isotropic liquid or disordered phase;

ii) $\eta \neq 0$, $\tau = \sigma = 0$, orientational order characteristic of the nematic phase in accordance with the Maier Saupe theory;

iii) $\eta \neq 0$, $\tau \neq 0$, $\sigma \neq 0$, orientational and translational order characteristic of the smectic A phase.

Due to lack of other alternatives, the experimental data for the pure compounds having Smectic B phase have been fitted with those calculated from the McMillan's theory for Smectic A phase with the potential parameters α and δ as adjustable parameters.

2.15. Materials for VA mode applications:

2.15.1. Basic requirement and physical properties:

For commercial applications, a broad nematic range of the liquid crystalline material from -40 to 100°C is required in order to guarantee the so called operating temperature range of LCD's [99]. Furthermore, the clearing temperature of the mixture should be at least 10°C higher than the operating temperature of the device.

The magnitude of the dielectric anisotropy $\Delta\varepsilon$, directly determines the strength of interaction of the liquid crystal with an applied electric field and therefore has a major influence on the threshold voltage. Depending on the molecular structure the dielectric anisotropy can be positive (molecular dipole parallel to the long axis of the molecule) or negative (molecular dipole perpendicular to the long axis of the molecule). Vertically Aligned (VA) mode applications require liquid crystalline materials with negative dielectric anisotropy. Such features are realized with LC's having lateral polar substituent which induce a dipole moment perpendicular to the long axes of the molecule. The standard Thin Film Transistor (TFT) driver requires an operating voltage under 6 volts. As a consequence the dielectric anisotropy of the LC mixture has to be around – 3 after taking the elastic constants into consideration.

Elastic constants K_{ii} (i = 1, splay, i = 2, twist and i = 3, bend), are the proportionality constants between the force (electric or magnetic) and the deformation of director fields. The operating voltage in a VA mode device is proportional to the square root of the fraction between the bend elastic constant and dielectric anisotropy. It is thus required to have materials with low values of the bend elastic constant. The variation of elastic constants in ideal mixtures has been found to be almost linear for the splay and the twist elastic constants. However, the bend elastic constant K_{33} shows a negative deviation and its behaviour is difficult to predict.

For VA mode applications, the required optical path length (d.Δn) is around 0.3μm. For currently used cell gaps (≈ 4μm), this requires a birefringence values for the VA mixtures to be around 0.08 [99].

Furthermore, due to the increasing number of moving picture internet applications and the overlap of monitor – video and TV technology, the reduction of switching times is another very important issue for liquid crystal material development. The switching time of 25 ms from black to white state for VA LCDs is not sufficient to realize full moving pictures. To achieve at least 90% transition between two frames switching time of 16msec (i.e. the time of one frame during which the voltage is sustained until the next refresh signal pulse arrives; for 60 Hz refresh rate) is the basic requirement. This necessitates the development of improved LC materials with lower rotational viscosity.

2.15.2. Structure-property relation:

All structural elements such as side chain, rings, linkage groups and terminal group etc. of a liquid crystal molecule contribute to the physical properties. For example benzene rings with polar substituents contribute to the dielectric anisotropy significantly. In addition, the aromatic ring contributes to higher values of the optical anisotropy (Δn) compared to a cyclohexane ring. As a consequence there are limitations for high polar liquid crystals with low Δn values. Other contradictory requirements are the simultaneous existence of high clearing point and low viscosity and materials with high polarity and low viscosity. Additional properties like solubility etc. also play a decisive role for practical use. Moreover, liquid crystals must be chemically, photochemically and electrochemically stable. Empirically, the Voltage Holding Ratio (VHR) [100-102], (VHR is defined to be the ratio of RMS voltage at a pixel within one-frame time period and initial voltage value) values decrease with

increasing dielectric anisotropy of the LCs. The combination of high polarity with high VHR is therefore another usually contradictory material requirement.

2.15.3. Structure and chemical name of the pure compounds as components of VA mode mixtures:

The applied materials that have been mainly used are the 2,3-difluoro sub-unit liquid crystalline compounds [6] having low rotational viscosity and broad phase transition temperature. Additionally, the physical properties of few bicyclohexane compounds, which have been used as additives in the multicomponent mixtures to adjust the birefringence, have also been studied. All the samples have been procured from AWAT Co., Warsaw, Poland and were used without further purification. The chemical structures and transition temperatures of the liquid crystals studied are listed in Table 2.1.

Table 2.1. Chemical structure and transition temperatures of the pure liquid crystals studied:

Sl. No.	Chemical Structure	T_m (^{0}C)	T_{SmB-N} (^{0}C)	T_{NI} (^{0}C)
1	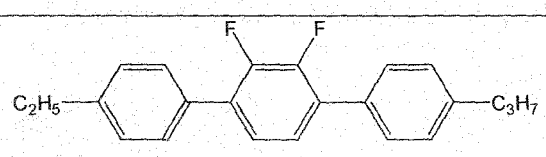	73	-----	110
2	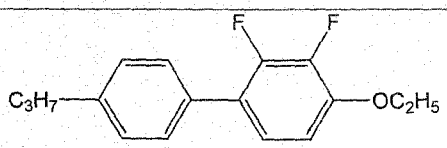	---	-----	50.3
3	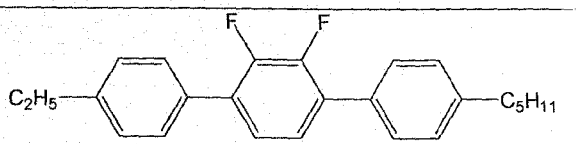	72.7	-----	114.5
4	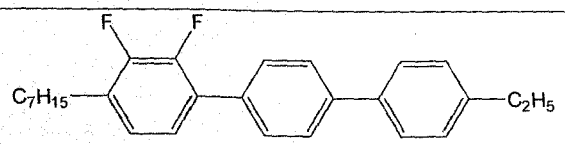	67.1	75.2	124.6

5	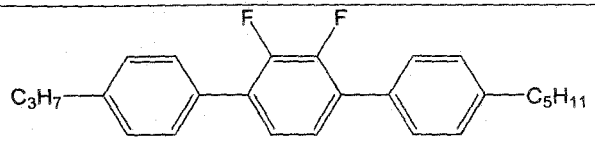	54.6	-----	123.1
6	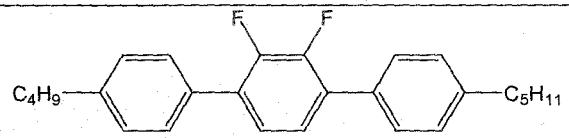	50.8	-----	111.6
7	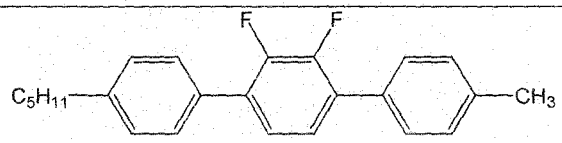	74.2	-----	128.1
8	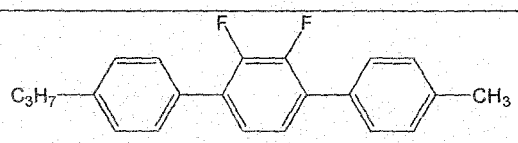	90.6	-----	132.7
9	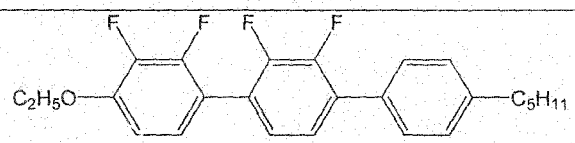	93.3	-----	122.9
10	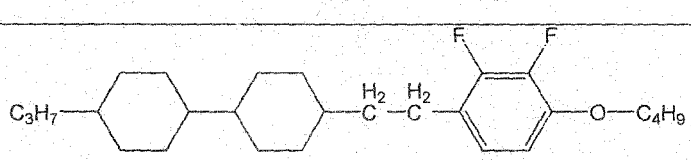	112	(110)	152
11	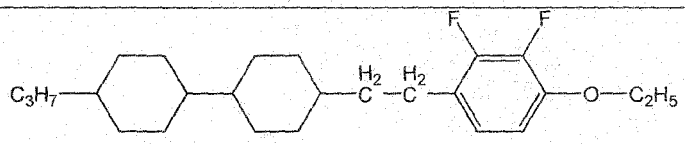	111	(109)	162
12	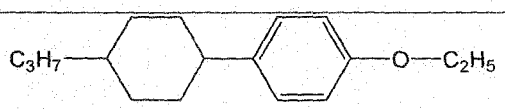	32	-----	37
13	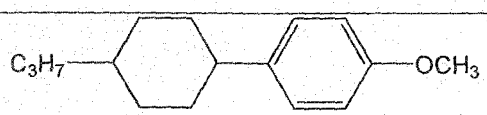	----	-----	33
14	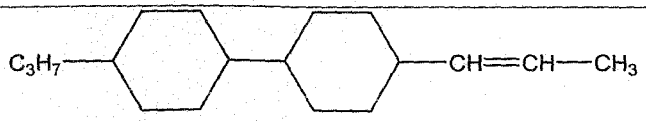	80	-----	86.4
15	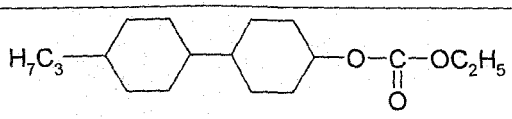	35	59.2	70
16	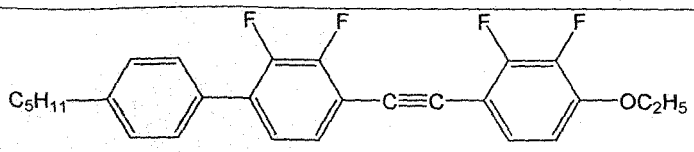	75.4	-----	195.5

17	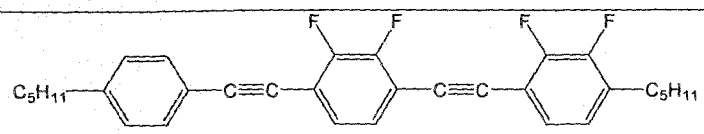	86.1	-----	171.8
18	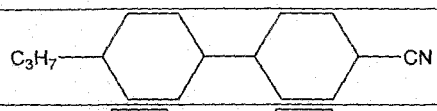	56.5	53.4	84
19	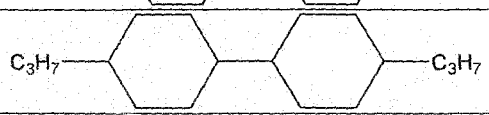	68.7	--	80.8
20	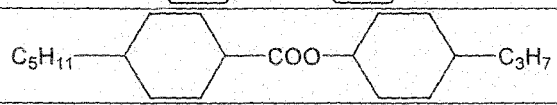	--	--	53
21	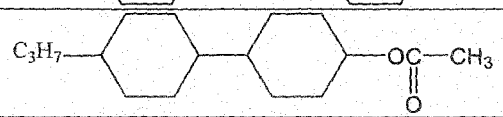	55.4	--	88.5
22	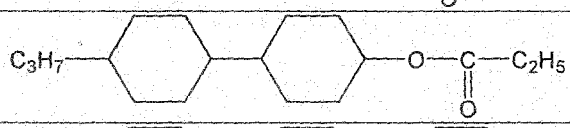	34.8	--	68.8
23	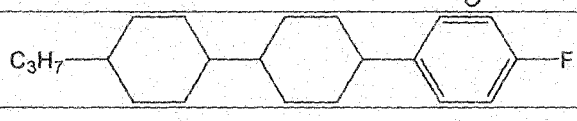	84.7	81.2	158

References:

[1] T. Kosaka, H. Tsubota, S. Kobayashi, T. Shimomura and R. Mozoguchi, *Proc. SID,* ***24***, 263 (1983); *SID Digest*, 174 (1982).

[2] S. Kobayashi, *Proc. Japan Display*, 198 (1983).

[3] M. Schadt and W. Helfrich, *Appl. Phys. Lett.*, ***13***, 155 (1971).

[4] G.H. Heimeir, L.A. Zannoni and L.A. Barton, *Appl. Phys. Letts.*, ***13***, 46 (1968).

[5] M.F. Schiekel and K. Fahrenschon, *Appl. Phys. Letts.*, *19*, 391 (1971).

[6] V. Reiffenrath, J. Krause, H.J. Plach, G. Weber, *Liq. Cryst.*, ***5***, 159 (1989).

[7] P. Kirsch and M. Bremer, *Angew. Chem.*, ***112***, 4384 (2000).

[8] P. Kirsch and M. Bremer, *Angew. Chem., Int. Ed.,* ***39***, 4216 (2000).

[9] Liquid crystalline medium and electro-optical display element, *EP-A 1352943* (2002).

[10] M. Imai, H. Naito, M. Okuda and A. Sugimura, *Mol. Cryst. Liq. Cryst.*, 259, 37 (1995).

[11] G.D. Lee *et al.*, *Appl. Phys. Lett.*, ***90***, 033509 (2007).

[12] H. Wang , T.X. Wu, X. Zhu and S.T. Wu., *Jounal of Applied Physics*, ***95***, 10 (2004).

[13] P.J. Martin, *Recent Patents on Material Science.*, *1*, 21 (2008).

[14] B. Bahadur, *Liquid crystals: Applications and Uses*, World Scientific: Singapore,Vol. I (1991).

[15] P.G. de Gennes and J. Prost, *The Physics of Liquid Crystals*, Clarendon Press, Oxford (1993).

[16] S. Charandrasekhar, *Liq. Cryst.*, Cambridge University Press, Cambridge (1977).

[17] A. Saupe and W. Maier, *Z. Natureforsch*, ***14a***, 882 (1959) and ***15a***, 287 (1960).

[18] (i) W.L. McMillan, *Phys. Rev.*, ***A4***, 1238 (1971) and (ii) W.L. McMillan, *Phys. Rev. A*, ***6***, 93 (1972).

[19] M. Schadt, R. Buchecker and K. Miiller, *Liq. Cryst.*, ***5***, 293 (1989).

[20] J. Szulc, Z. Witkiewicz and R. Dabrowski, *Mol. Cryst. Liq. Cryst.*, ***109***, 25 (1984).

[21] I. Z. Schröder, *Phys. Chem., 11*, 449 (1893).

[22] E.C.H. Hsu, J.F. Johnson, *Mol. Cryst. Liq. Cryst.*, ***20***, 177, (1973).

[23] G.R.V. Hecke, *The Journal of Physical Chemistry*, ***89 (10)***, 2058 (1985).

[24] H. Zocher, *Z.Krist.*, ***79***, 122 (1931).

[25] B. Adhikari and R. Paul, *Phase transitions*, ***56***, 165 (1996).

[26] M. Mitra, S. Gupta, R. Paul and S. Paul, *Mol. Cryst. Liq. Cryst.*, ***199***, 257 (1991).

[27] R. Chang, *Mol. Cryst. Liq. Cryst.*, ***30***, 155 (1975).

[28] G. Pelzl and H. Sackmann, *Symp. Faraday Soc.*, ***5***, 68 (1971).

[29] Y. Galerne, S.T. Lagerwall and I.W. Smith, *Opt. Commun.*, ***19***, 147 (1976).

[30] S.K. Sarkar and M.K. Das, *RSC Advances*, ***4 (38)***, 19861 (2014).

[31] D. Demus and L. Richter, *"Textures of Liquid Crystals"*, Verlag Chemie, New York (1978).

[32] A. Prasad and M.K. Das, *Phys. Scr.*, ***84***, 015603 (2011).

[33] P. Galatola and C. Oldano, *Optics of Thermotropic Liquid Crystals*, (Chapter 3) Eds. S. Elston and R. Sambles, Tailor and Francis (1998).

[34] E. Dorn, *Phys. Z.*, ***11***, 777 (1910).

[35] H. Zocher, *Trans. Faraday Soc.*, ***29***, 931 (1933).

[36] H.E. Neugebauer, *Canad. J. Phys.*, ***32***, 1 (1954).

[37] M.F. Vuks, *Optics and Spectroscopy*, ***20***, 361 (1966).

[38] A.K. Zeminder, S. Paul and R. Paul, *Mol. Cryst. Liq. Cryst.*, ***61***, 191 (1980).

[39] S.K. Sarkar and M.K. Das, *International Journal of Research in Applied, Natural and Social Sciences*, ***1(4)***, 1 (2013).

[40] A. Saipa and F. Gisselmann, *Liq. Cryst.*, ***29***, 347 (2002).

[41] T. Scharf, *Polarized Light in Liquid Crystals and Polymers* (Hoboken, NJ: Wiley) (2007).

[42] G. Sarkar, B. Das, M.K. Das and W. Weissflog, *Phase Transitions*, ***82***, 433 (2009).

[43] A. Prasad and M.K. Das, *J. Phys.: Condens. Matter*, ***22***, 195106 (2010).

[44] I. Haller, H. A. Huggins, H. R. Lilienthal and T. R. McGuire, J. Phys. Chem., *77*, 950 (1973).

[45] B.J. Zywucki and W. Kuczynski, *IEEE Trans. Dielectr. Electr. Insul.*, ***8***, 512 (2001).

[46] W. Kuczynski, B. Zywucki, and J. Malecki, *Mol. Cryst. Liq. Cryst.*, ***381***, 1 (2002).

[47] M. Geppi, A. Marini, B. Mennucci, P. Kula, A. Spadlo, W. Kuczynski and S. Urban, *Mol. Cryst. Liq. Cryst.*, ***541***, 104 (2011).

[48] P. Pardhasaradhi, P.V.D. Prasad, D.M. Latha, V.G.K.M. Pisipati and G.P. Rani, *Phase Trans.*, ***85***, 1031 (2012).

[49] K.D. Thingujama, P.R. Alapati, B. Choudhury and A. Bhattacharjee, *Phase Trans.*, ***85***, 52 (2012).

[50] K. Fakruddin, R.J. Kumar, P.V.D. Prasad and V.G.K.M. Pisipati, *Mol. Cryst. Liq. Cryst.*, ***511***, 133 (2009).

[51] E.G. Hanson and Y.R. Shen, *Mol. Cryst. Liq. Cryst.*, ***36***, 193 (1976).

[52] A. Kumar, *Liq. Cryst.*, ***40***, 203 (2013).

[53] V.G.K.M. Pisipati and P.V.D. Prasad, *Mol. Cryst. Liq. Cryst.*, ***506***, 13 (2009).

[54] M.S. Zakerhamidi and H. Rahimzadeh, *Mol. Cryst. Liq. Cryst.*, ***569***, 92 (2012).

[55] S.S. Sastry, S. Kumar, T.V. Kumari, K. Mallika, B. Gowri, S. Rao and H.S. Tiong, *Liq. Cryst.*, ***39***, 1527 (2012).

[56] S.S. Sastry, T.V. Kumari, K. Mallika, B.G.S. Rao, S. Ha and S. Lakshminarayana, *Liq. Cryst.*, ***39***, 295 (2012).

[57] M.K. Das, G. Sarkar, B. Das, R. Rai and N. Sinha, *J. Phys.: Condens. Matter*, ***24***, 115101(2012).

[58] G. Sarkar, B. Das, M. K. Das, U. Baumeister and W. Weissflog, *Mol. Cryst. Liq. Cryst.*, ***540 (1)***, 188 (2011).

[59] H. Zöcher, *Trans. Faraday Soc.*, ***29***, 945 (1933).

[60] C.W. Oseen, *Ark. Mat. Astron. Fys.*, ***19A***, 1 (1925).

[61] C.W. Oseen, *Trans. Faraday Soc.*, ***29***, 883 (1933).

[62] F.C. Frank, *Discuss. Faraday Soc.*, ***25***, 19 (1958).

[63] J.L. Ericksen, *Phys. Fluids*, ***9***, 1205 (1966).

[64] A. Dunmur, A. Fukuda and G.R. Luckhurst, *Physical Properties of Liquid Crystal Nematics*, INSPEC publications, London, U.K. (2001).

[65] V. Freedericksz and V. Zolina, *Trans. Faraday Soc., 29(1)*, 919 (1933).

[66] H. Gruler, T.J. Schiffer and G. Meier, *Z. Natureforsh.*, ***27a***, 966 (1972).

[67] H. Gruler and L. Cheung, *J. Appl. Phys.*, ***46***, 5097 (1975).

[68] L. Pohl and U. Finkenzeller in B. Bahadur (Ed.) *Liquid Crystals, Application and Uses*, Vol. 1, World Scientific, 166 (1990).

[69] M.J. Bradshaw and E.P. Rayens, *Mol. Cryst. Liq. Cryst.*, ***72***, 35 (1980).

[70] P.P. Karat and N.V. Madhusudana, *Mol. Cryst. Liq. Cryst.*, ***40***, 239 (1977).

[71] H.P. Schad and M.A. Osman, *J. Chem. Phys.*, ***75 (2)***, 880 (1981).

[72] F.Leenhouts, H.J.Boeber, A.J.Dekker and J.J.Jonker, J. *Phys. (Paris) Colloque.*, ***40***, C3-291 (1979).

[73] H.P. Schad, G. Bauer and G. Maier, *J. Chem. Phys.*, ***67***, 3705 (1977).

[74] P. Dasgupta, B. Das and M.K. Das, *Liq. Cryst.*, ***39 (11)***, 1297 (2012).

[75] F. Leenhouts and A.J. Dekker, *J. Chem. Phys.*, ***74***, 1956 (1981).

[76] H.J. Deuling, *Liq. Cryst. Sol. State. Phys. Suppl.*, ***14***, 77 (1978).

[77] V. Freedericksz and V. Tsvetkov, *Phy. Z. Soviet Union.*, ***6***, 490 (1933).

[78] S.T. Wu and C.S. Wu, *Phys. Rev. A*, ***42***, 2219 (1990).

[79] M.L. Dark, M.H. Moore, D.K. Shenoy and R. Shashidhar, *Liq. Cryst.*, 33, 67 (2006).

[80] M.K. Das, A. Pramanik, B. Das, L. Szczucinski and R. Dabrowski, *J.Phys. D: Appl. Phys.*, ***45***, 415304 (2012).

[81] A. Pramanik, B. Das, M.K. Das, K. Garbat, S. Urban and R. Dabrowski, *Liq. Cryst.*, ***40***, 149 (2013).

[82] A. Chakraborty, M.K. Das, B. Das, A. Lehmann and C. Tschierske, *Soft Matter*, ***9***, 4273 (2013).

[83] S. Gauza, M. Jiao, S.T. Wu, P. Kula, R. Dabrowski and S. Liang, *Liq. Cryst.*, ***35(12)***, 1401 (2008).

[84] T.N. Ruckmongathan, T. Kuwata, T. Ohnishi, S. Ihara, H. Koh and Y. Nakagawa, *Japan Display '92.* 65 (1992).

[85] T.N. Ruckmongathan, *Reports Res. Lab. Asahi Glass Co. Ltd., 43(1)*, 65 (1993).

[86] W.H. de Jue, *Physical Properties of Liquid Crystalline Materials;* Gordon and Breach Science Publishers: London, (1980).

[87] E. Otón, S. López-Andrés, C. Carrasco-Vela, B. Cerrolaza, N. Bennis, and J. Manuel Otón, *Journal of Display Technology*, ***6(7)***, 2010.

[88] B.K.Vainshtein and I.G.Chistyakov, *Problem of Modern Crystallography*, Nauka, Moscow (1975).

[89] A.J. Leadbetter, *The Molecular Physics of Liquid Crystals*, Eds. G.R. Luckhurst & G.W. Gray, Chap.13, Academic Press (1979).

[90] A.J. Leadbetter and E.K. Norris, *Mol. Phys.*, ***38***, 669 (1979).

[91] H. Kohli *et al.*, *Z. Physik*, ***B24***, 147 (1976).

[92] A. de Vries, *J. Chem. Phys.*, ***56***, 4489 (1972).

[93] A. de Vries, *Mol. Cryst. Liq. Cryst.*, ***10***, 219 (1970).

[94] B. Jha and R. Paul, *Proc. Nucl. Phys. Solid State Phys. Symp., India*, ***19c***, 491 (1970).

[95] H.P. Klug and L.E. Alexander, *X-ray diffraction procedures*, John Wiley and Sons, NewYork, 114 and 473 (1974)

[96] R.L. Humphries, G. James and G.R. Luckhurst, *Chem. Soc. Faraday Trans II*, ***68***, 1031 (1972)

[97] K. Kobayashi, *J. Phys. Soc. (Japan)*, ***29***, 101 (1970).

[98] K. Kobayashi, *Mol. Cryst. Liq. Cryst.*, ***13***, 137 (1971).

[99] D. Pauluth and K. Tarumi, *J. Matter. Chem.*, ***14***, 1219 (2004).

[100] V. Reiffenrath, J. Krause, A. Wachtler, G. Weber and U. Finkenzeller *(Merck KgaA)*, EP-B0364538 (1988).

[101] P. Kirsch, V. Reiffenrath and M. Bremer, *Synlett.*, **4,** 389 (1999).

[102] M. Klasen, M. Bremer and K. Tarumi, *Jpn. J. Appl. Phys.*, ***39***,1180 (2009).